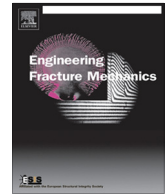




ELSEVIER

Contents lists available at ScienceDirect

## Engineering Fracture Mechanics

journal homepage: [www.elsevier.com/locate/engfracmech](http://www.elsevier.com/locate/engfracmech)

# Modeling of multiple crack propagation in 2-D elastic solids by the fast multipole boundary element method

Y.J. Liu <sup>a,b,\*</sup>, Y.X. Li <sup>a</sup>, W. Xie <sup>b</sup><sup>a</sup> Mechanical Engineering, University of Cincinnati, P.O. Box 210072, Cincinnati, OH 45221-0072, USA<sup>b</sup> Institute for Computational Mechanics and Its Applications, Northwestern Polytechnical University, Xi'an, Shaanxi 710072, PR China

## ARTICLE INFO

## Article history:

Received 8 October 2016

Received in revised form 8 December 2016

Accepted 6 January 2017

Available online 9 January 2017

## Keywords:

Crack propagation

Multiple cracks

Boundary element method

Fast multipole method

## ABSTRACT

In this paper, a fast multipole boundary element method (BEM) is presented for modeling crack propagation in two-dimensional (2-D) linear elastic solids. A dual boundary integral equation (BIE) formulation using a linear combination of the displacement and traction BIEs is applied to model cracks in this BEM. Constant boundary elements are used to discretize the BIEs and the fast multipole method (FMM) is applied to accelerate the solution of the BEM system of equations. Numerical examples of multiple crack propagation in 2-D elastic domains and under cyclic loading, including perforated plates with multiple holes and cracks, are presented to show the effectiveness and efficiency of the developed fast multipole BEM.

© 2017 Elsevier Ltd. All rights reserved.

## 1. Introduction

The boundary element method (BEM) based on the boundary integral equation (BIE) for elasticity theory [1] has been applied to solve crack problems for more than three decades (see, e.g., some reviews in Refs. [2–9]). The multidomain BEM was first introduced to solve crack problems [10] using only the displacement (singular) BIE, in which a cracked body is divided into subdomains using artificial boundaries connecting the cracks. In the late of 1980s and early 1990s, the traction (hypersingular) BIE [11–17] was introduced and the displacement discontinuity (or jump) across the crack surfaces is used as the primary unknown variable to solve the crack problems based on the one crack surface model. This one crack surface formulation using the traction BIE only has been shown to be equivalent to the displacement discontinuity method (DDM) proposed by Crouch in 1976 [18], when constant elements are applied for both 2-D and 3-D cases [19–21]. Since then, various dual BIE formulations [22–28] using different combinations of the displacement and traction BIEs have been applied to solve crack problems in more general settings. The BEM has also been applied successfully in modeling interface cracks and cracks in functionally-graded materials (e.g., [29–33]). More comprehensive reviews of the BEM for modeling crack problems can be found in Refs. [5,6,9].

Although the BEM is accurate in solutions and efficient in meshing for solving crack problems, the computational efficiency had been a huge hurdle for the method for a long time, as the BEM system of equations is dense and nonsymmetrical. With a direct equation solver, both the computing time and memory storage are of at least  $O(N^2)$  complexity (with  $N$  being the number of unknowns). To improve the computational efficiency, the fast multipole method (FMM) pioneered by Rokhlin and Greengard [34–36] has been introduced in the BEM to solve the crack problems. Many large-scale BEM models of mul-

\* Corresponding author at: Mechanical Engineering, University of Cincinnati, P.O. Box 210072, Cincinnati, OH 45221-0072, USA.

E-mail address: [Yijun.Liu@uc.edu](mailto:Yijun.Liu@uc.edu) (Y.J. Liu).

multiple cracks have been solved successfully using the fast multipole BEM in static and dynamic load cases [37–45], as well as in the modeling of crack propagations [46]. Detailed reviews and discussions of the fast multipole BEM can be found in Refs. [9,37,47,48].

In this work, a new fast multipole BEM for modeling large-scale 2-D linear elastic fracture mechanics problems is presented. A dual BIE formulation using a linear combination of the displacement and traction BIEs is applied on all boundaries of the problem domain, including surfaces of the cracks. This dual BIE formulation was originated by Burton and Miller [49] for solving exterior acoustic wave problems to remove the fictitious eigenfrequencies in the BIE solutions, which has also been found very effective in solving crack problems in the context of potential theory, acoustics and elastodynamics [26,27,50,51]. Due to the use of the hypersingular BIE which requires  $C^1$  continuity of the field at the collocation point [52], higher-order elements or nonconforming elements have been applied in those works [26,27,50,51]. In this work, however, constant boundary elements are used to discretize the dual BIEs. Good numerical results have been obtained in determining the stress intensity factors (SIFs) using constant elements for 2-D crack problems [45]. This work will further show that the dual BIE formulation discretized with constant elements can also be applied successfully to model crack propagation problems with the fast multipole BEM. Numerical examples of propagation of multiple cracks in perforated plates with many holes are given in this paper to show the effectiveness and efficiency of the developed fast multipole BEM.

## 2. BIE formulation

We first review the direct BIE formulation for modeling crack problems under static loading. We start with the following direct displacement BIE (conventional BIE or CBIE) for a 2-D elastic body containing cracks [1]:

$$\frac{1}{2}\mathbf{u}(\mathbf{x}) = \int_S [\mathbf{U}(\mathbf{x}, \mathbf{y})\mathbf{t}(\mathbf{y}) - \mathbf{T}(\mathbf{x}, \mathbf{y})\mathbf{u}(\mathbf{y})]dS(\mathbf{y}), \quad \forall \mathbf{x} \in S, \quad (1)$$

where  $S$  is the entire boundary of the problem domain (including all crack surfaces and the outer boundary of the domain, if present);  $\mathbf{x}$  and  $\mathbf{y}$  are the source point and field point, respectively;  $\mathbf{u}$  and  $\mathbf{t}$  are the displacement and traction vector, respectively;  $\mathbf{U}$  and  $\mathbf{T}$  are  $2 \times 2$  matrices from the displacement and traction kernels in the Kelvin's solution, respectively [37]. It is assumed that the surface is smooth at the source point  $\mathbf{x}$ . For completeness, we list the expressions for the two kernels ( $\mathbf{U}$  and  $\mathbf{T}$ ) in index notation for the plane strain condition [37]:

$$U_{ij}(\mathbf{x}, \mathbf{y}) = \frac{1}{8\pi\mu(1-\nu)} \left[ (3-4\nu)\delta_{ij} \log\left(\frac{1}{r}\right) + r_{,i}r_{,j} \right], \quad (2)$$

$$T_{ij}(\mathbf{x}, \mathbf{y}) = -\frac{1}{4\pi(1-\nu)r} \left\{ \frac{\partial r}{\partial n} [(1-2\nu)\delta_{ij} + 2r_{,i}r_{,j}] - (1-2\nu)(r_{,i}n_j - r_{,j}n_i) \right\}, \quad (3)$$

in which  $\mu$  is the shear modulus,  $\nu$  is Poisson's ratio,  $r$  is the distance between the source point  $\mathbf{x}$  and field point  $\mathbf{y}$ ,  $(\ )_{,i} = \partial(\ )/\partial y_i$ ,  $\delta_{ij}$  is the Kronecker  $\delta$  symbol, and  $n_i$  is the direction cosine of the normal.

For a crack with two surfaces denoted as  $S^+$  and  $S^-$  (Fig. 1), if we let  $S^-$  collapse onto  $S^+$  to form a one surface model for the crack, the displacement BIE (1) collocated on the crack surface  $S^+$  is reduced to the following [26,53]:

$$\frac{1}{2}\Sigma\mathbf{u}(\mathbf{x}) = \int_{S^+} [\mathbf{U}(\mathbf{x}, \mathbf{y})\Sigma\mathbf{t}(\mathbf{y}) - \mathbf{T}(\mathbf{x}, \mathbf{y})\Delta\mathbf{u}(\mathbf{y})]dS(\mathbf{y}), \quad \forall \mathbf{x} \in S^+, \quad (4)$$

where  $\Delta\mathbf{u} = \mathbf{u}|_{S^+} - \mathbf{u}|_{S^-}$ ,  $\Sigma\mathbf{u} = \mathbf{u}|_{S^+} + \mathbf{u}|_{S^-}$ , and  $\Sigma\mathbf{t} = \mathbf{t}|_{S^+} + \mathbf{t}|_{S^-}$ . Additional terms from integrals on the outer boundary or other crack surfaces may appear on the right-hand side of the equation. Note that Eq. (4) is insufficient when it is applied alone to solve a crack problem, as it contains both the displacement sum and displacement discontinuity across the crack surfaces (There are two unknown functions). Therefore, the traction (hypersingular) BIE was introduced in late of 1980s in the BEM for modeling crack problems. The direct traction BIE (hypersingular BIE or HBIE) is [7,22,37]:

$$\frac{1}{2}\mathbf{t}(\mathbf{x}) = \int_S [\mathbf{K}(\mathbf{x}, \mathbf{y})\mathbf{t}(\mathbf{y}) - \mathbf{H}(\mathbf{x}, \mathbf{y})\mathbf{u}(\mathbf{y})]dS(\mathbf{y}), \quad \forall \mathbf{x} \in S, \quad (5)$$

where  $\mathbf{K}$  and  $\mathbf{H}$  are  $2 \times 2$  matrices from the two new kernels in the Kelvin's solution [37]. The two kernels ( $\mathbf{K}$  and  $\mathbf{H}$ ) for the case of plane strain are given in the following [37]:

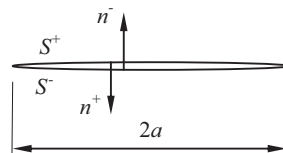


Fig. 1. A crack in a 2-D elastic domain (crack surface  $S = S^+ \cup S^-$ ).

$$K_{ij}(\mathbf{x}, \mathbf{y}) = \frac{1}{4\pi(1-\nu)r} [(1-2\nu)(\delta_{ij}r_{,k} + \delta_{jk}r_{,i} - \delta_{ik}r_{,j}) + 2r_{,i}r_{,j}r_{,k}]n_k(\mathbf{x}), \quad (6)$$

$$H_{ij}(\mathbf{x}, \mathbf{y}) = \frac{\mu}{2\pi(1-\nu)r^2} \left\{ 2 \frac{\partial r}{\partial n} [(1-2\nu)\delta_{ik}r_{,j} + \nu(\delta_{ij}r_{,k} + \delta_{jk}r_{,i}) - 4r_{,i}r_{,j}r_{,k}] + 2\nu(n_i r_{,j} r_{,k} + n_k r_{,i} r_{,j}) \right. \\ \left. - (1-4\nu)\delta_{ik}n_j + (1-2\nu)(2n_j r_{,i} r_{,k} + \delta_{ij}n_k + \delta_{jk}n_i) \right\} n_k(\mathbf{x}). \quad (7)$$

When  $S^-$  is collapsed onto  $S^+$  to form a one surface model for a crack, the traction BIE (5) is reduced to the following [7,13–15,24–27]:

$$\frac{1}{2} \Delta \mathbf{t}(\mathbf{x}) = \int_{S^+} [\mathbf{K}(\mathbf{x}, \mathbf{y}) \Sigma \mathbf{t}(\mathbf{y}) - \mathbf{H}(\mathbf{x}, \mathbf{y}) \Delta \mathbf{u}(\mathbf{y})] dS(\mathbf{y}), \quad \forall \mathbf{x} \in S^+, \quad (8)$$

where  $\Delta \mathbf{t} = \mathbf{t}|_{S^+} - \mathbf{t}|_{S^-}$ . Traction BIE (8) is ideal for solving the displacement discontinuity (or jump) for crack problems (Fig. 2a), which can then be applied to calculate the stress intensity factors, when the traction is specified on the crack surfaces or load at other boundaries are given. For pure crack problems, for example, multiple cracks in an infinite elastic domain (no outer boundary), this approach (Fig. 2a) using the HBIE (8) only is also more efficient as it contains only displacement discontinuity and only one surface needs to be discretized for each crack. Therefore, the number of unknowns can be reduced by one half in the BEM based on HBIE (8).

However, for more general cases, such as structures containing both cracks and voids, and within a finite domain with loads applied on the outer boundary, general forms of the displacement BIE (1) and traction BIE (5) need to be applied. This is the emergence of the so called dual BIE formulations for crack problems [5–7,26–28]. Fig. 2b shows the most commonly used dual BIE approach [25] in the literature for modeling cracks using the two-surface models. In this approach, the displacement BIE (CBIE) is collocated on one side of the crack, and the traction BIE (HBIE) is collocated on the other. The CBIE is also applied on other non-crack surfaces. This dual BIE approach has been applied in many works for modeling crack propagation problems.

Another dual BIE approach is shown in Fig. 2c, which uses a linear combination of the CBIE and HBIE as follows:

$$\text{CBIE} + \beta \text{HBIE} = 0, \quad (9)$$

where  $\beta$  is a coupling coefficient. This dual BIE formulation, which is applied to the entire boundary (including all crack surfaces), was originally proposed by Burton and Miller [49] for solving exterior acoustic wave problems to overcome the fictitious eigenfrequency difficulties in the BIEs. We have applied this dual BIE formulation in solving crack problems in 3-D elastodynamics [27] and 2-D elastostatics for calculating SIFs [45]. In those earlier studies, the coupling coefficient  $\beta$  was chosen to be a constant for a given BEM model. This dual BIE approach is easier to implement, as one does not need to distinguish the two crack surfaces, and the other boundary surfaces. The same dual BIE formulation is applied uniformly throughout the model, and therefore the BEM input data is also simplified. In addition, better conditioning of the BEM matrices can be expected, as the scales of the coefficients computed from the two crack surfaces are in the same order. This is in contrast to the dual BIE using the CBIE on one side of the crack and the HBIE on the other (Fig. 2b), where the coefficients can have differences of several orders in values if real material constants are used in the BEM model.

In this study, we propose a new adaptive coefficient  $\beta$  in the dual BIE formulation (9), which is found to be more efficient than using a constant  $\beta$ . The following formula is used to determine the value of  $\beta$  at each collocation point  $\mathbf{x}$ :

$$\beta = \beta(\mathbf{x}) = \frac{h(\mathbf{x})}{E}, \quad (10)$$

where  $h(\mathbf{x})$  is the size of the element on which the collocation point  $\mathbf{x}$  is located, and  $E$  is the Young's modulus. The rationale behind this choice is that traction BIE (5) is obtained by taking the derivatives of the displacement BIE (1) and multiplying the results by the Young's modulus tensor. Therefore, in order to make the two terms in dual BIE (9) have the same unit and order of magnitude, choice of  $\beta$  as given in Eq. (10) seems to be a natural one.

Constant line elements are applied in the discretization of dual BIE (9) for modeling cracks in 2-D, and the solution of the BEM system of equations is accelerated by the fast multipole method (see Refs. [37,54] for details). The constant elements have been shown to be able to provide results of the SIFs within 1% of accuracy for various verification cases [45]. The use of constant elements with the traction BIE has also been shown [19–21] to be equivalent to the displacement discontinuity method [18], which has been used widely in rock mechanics for modeling cracks. Although constant elements have lower accuracy compared with the linear or quadratic elements, they do offer many advantages, including: (1) They are easier to implement as analytical integration of all integrals are readily available in the literature (e.g., Ref. [37]) and therefore no numerical integration is needed; (2) The smoothness requirement on the HBIE [52] is satisfied at the collocation points; and (3) No need to deal with any corner problems. In this study, the crack-tip opening displacement (CTOD) is used in evaluating the SIFs, which are used to determine the propagation direction of each crack tip. For completeness, the formulas in fracture mechanics used in this work are summarized in the subsequent section.

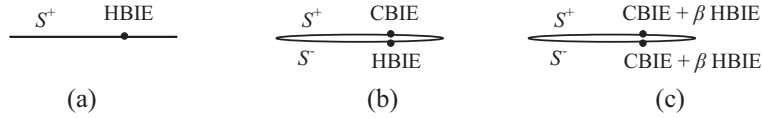


Fig. 2. Three different approaches in modeling cracks by using the BIEs.

### 3. Formulas for determining crack propagation direction

First, the following formulas are used to compute the stress intensity factors:

$$K_I = \frac{\mu}{1 + \kappa} \sqrt{\frac{2\pi}{r}} \Delta v, \quad K_{II} = \frac{\mu}{1 + \kappa} \sqrt{\frac{2\pi}{r}} \Delta u, \quad (11)$$

for mode I and mode II, respectively, in which  $\kappa = 3 - 4\nu$  for plane strain, and  $\kappa = (3 - \nu)/(1 + \nu)$  for plane stress. These formulas are evaluated at nodes near the crack tip and in the local coordinate system  $xy$  (Fig. 3).

Then, the crack propagation angle (turning angle)  $\theta$  (Fig. 3) is determined from the following equation:

$$K_I \sin \theta + K_{II}(3 \cos \theta - 1) = 0. \quad (12)$$

We apply the following formula for  $\theta$ , which is a solution of the above equation:

$$\theta = 2 \tan^{-1} \left( \frac{K_I - \sqrt{K_I^2 + 8K_{II}^2}}{4K_{II}} \right) = 2 \tan^{-1} \left( \frac{-2K_{II}}{K_I + \sqrt{K_I^2 + 8K_{II}^2}} \right). \quad (13)$$

The second expression in Eq. (13) is good when either  $K_I = 0$  or  $K_{II} = 0$  (but not both).

The effective stress intensity factor  $K_{eff}$  of each crack tip is given by

$$K_{eff} = K_I \cos^3 \left( \frac{\theta}{2} \right) - 3K_{II} \cos^2 \left( \frac{\theta}{2} \right) \sin \left( \frac{\theta}{2} \right), \quad (14)$$

at each crack propagation step. If the maximum effective SIF is larger than the material toughness  $K_{IC}$ , then the analysis is stopped since unstable crack propagation will occur.

Under cyclic loading with constant amplitude, the fatigue crack growth rate can be determined by using the Paris law [55]:

$$\frac{da}{dN} = C \Delta K^m, \quad (15)$$

where  $a$  is the crack length,  $N$  is the number of load cycles, and  $C$  and  $m$  are two material constants.

In this study, we assume that the range of the applied cyclic load is from 0 to  $P$  (maximum value of the load). That is,  $K_{max} = K_{eff}$ , and  $K_{min} = 0$ , and therefore  $\Delta K = K_{eff}$ . Then, from the Paris law (Eq. (15)), the crack propagation length of each crack tip can be calculated using the following relation for multiple crack cases:

$$\Delta a_i = \left( \frac{K_{eff}^i}{K_{eff}^{max}} \right)^m \Delta a_{max}, \quad (16)$$

where  $\Delta a_i$  is the propagation length of the  $i$ th crack tip,  $K_{eff}^i$  is the effective SIF of the  $i$ th crack tip,  $K_{eff}^{max}$  is the maximum value of all  $K_{eff}^i$ , and  $\Delta a_{max}$  is the propagation length of the crack tip with  $K_{eff}^{max}$ . In this study,  $\Delta a_{max}$  is fixed and given for each analysis. In general, the chosen value of  $\Delta a_{max}$  should be smaller than 1/10th of the value of the original crack length, in order to have converged results of the computed crack propagation path [46,56,57]. With obtained  $\Delta a_i$  and  $\theta$ , each crack tip propagates accordingly in the following increment.

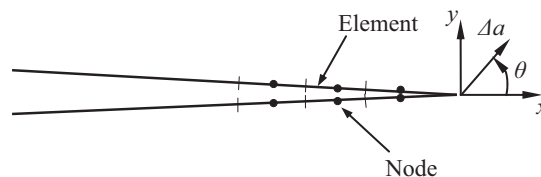


Fig. 3. Constant elements at a crack tip.

Six new elements (three on each crack surface) are added at each propagated crack tip for the following calculation. In addition, if the distance between a crack tip and the boundary of the domain or another crack surface is estimated to be smaller than the propagation length of that crack tip, then that crack tip will not propagate in the following increments.

#### 4. Numerical examples

Several examples of predicting propagation of cracks in 2-D elastic bodies are presented in this section to demonstrate the effectiveness and efficiency of the developed fast multipole BEM. In all the examples, the dual BIE (Fig. 2c) is applied with an adaptive  $\beta$  (Eq. (10)). Plane stress condition is assumed. The tolerance for convergence of the iterative solver used in the FMM is chosen to be 1.0E-5. The solutions were done on a Dell XPS 8900 desktop PC with an Intel® Core™ i7-6700 processor and 16 GB RAM.

##### 4.1. A plate with a center crack

A rectangular plate with a center crack of 8 mm long and an inclination of 45 deg, as shown in Fig. 4, is considered first. The plate is subjected to a cyclic tension load of 10 MPa on the top and constrained on the bottom. The Young's modulus is 72 GPa, Poisson's ratio is 0.33, fracture toughness is 3288.76 N/mm<sup>1.5</sup>, and  $\Delta a_{\max}$  is chosen to be 0.5 mm. There are 500 constant elements in the BEM model initially, of which 100 elements are on the crack surfaces. The predicted crack propagation paths after 35 incremental steps when the crack reaches the boundary of the plate using the FMM BEM and conventional BEM are shown in Fig. 5a and b, respectively, which are in good agreement, as expected. Fig. 5c shows the stress contour plot of  $\sigma_y$  after 16 increments of the propagation.

##### 4.2. A plate with two edge cracks

In this example, a rectangular plate with two 2 mm long edge cracks, which are offset by 2 mm vertically on the opposite sides, is considered (Fig. 6). A tension load of 10 MPa is applied on the top of plate, and the plate is supported on the bottom. The Young's modulus is 72 GPa, Poisson's ratio is 0.33, fracture toughness is 3288.76 N/mm<sup>1.5</sup>, and  $\Delta a_{\max}$  is 0.2 mm. The BEM mesh has 500 elements initially with 50 elements on each crack. Fig. 7a and b show the predicted propagation paths of the cracks after 58 increments of the cracks using the FMM BEM and conventional BEM, respectively. Again, both are in good agreement and they are consistent with results reported in the literature [58] or observed for similar cases. Fig. 7c shows the stress contour plot of  $\sigma_y$  after 27 increments of the propagation.

##### 4.3. A cracked plate with one hole

A rectangular plate with one hole of diameter 10 mm and one 6 mm long edge crack, as shown in Fig. 8, is studied next. A tension load of 10 MPa is applied on the top of plate, and the plate is fixed on the bottom. The Young's modulus is 72 GPa, Poisson's ratio is 0.33, fracture toughness is 3288.76 N/mm<sup>1.5</sup>, and  $\Delta a_{\max}$  is 0.7 mm. The BEM model has 500 elements initially with 50 elements on the crack and 50 elements on the hole. Fig. 9 shows comparison of the result of the propagation path of the crack after 45 increments of the crack using the FMM BEM and compared with the test result and XFEM result reported in Ref. [59]. Very good agreement among the BEM, experimental and XFEM results are observed.

##### 4.4. A cracked plate with four holes

A rectangular plate with four holes of diameter 10 mm and one 6 mm long edge crack, as shown in Fig. 10, is studied next. The plate is subjected to a tension load of 10 MPa and supported on the bottom. The Young's modulus is 72 GPa, Poisson's ratio is 0.33, fracture toughness is 3288.76 N/mm<sup>1.5</sup>, and  $\Delta a_{\max}$  is 0.8 mm. The mesh has 650 elements initially with 50 elements each on the crack and on each hole. Fig. 11 show the results of crack propagation path after 70 increments using the FMM BEM and conventional BEM, respectively. Fig. 11c shows the stress contour plot of  $\sigma_y$  after 68 increments of the propagation.

##### 4.5. A cracked plate with three holes

A rectangular plate [56,57] with three holes of diameter 12.7 mm and one 38.1 mm long edge crack is analyzed. The plate is subjected to a point load of 4.448 kN on the center of the top edge and boundary conditions shown in Fig. 12. The Young's modulus is 2.068 GPa, Poisson's ratio is 0.3, fracture toughness is 81.016 GPa $\sqrt{m}$  and  $\Delta a_{\max}$  is 2.2 mm. The initial mesh has 2340 elements with 100 elements on the crack and 200 elements on each hole. Fig. 13 shows the results of crack propagation path after 41 increments using the FMM BEM and compared with the test result and BEM result reported in Refs. [56,57]. Good agreement is observed in this case.

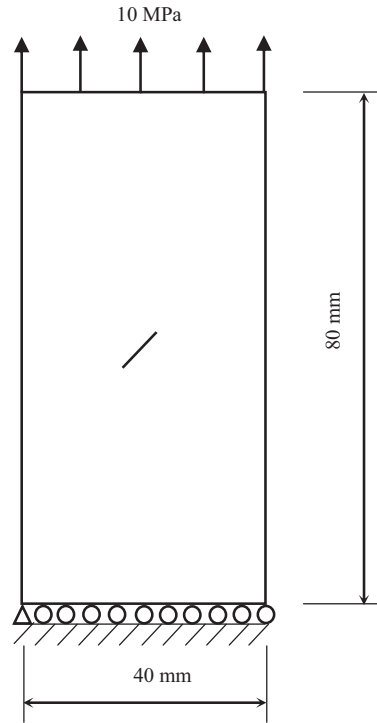


**Fig. 4.** A plate with a center crack (inclination of 45 deg and length of 8 mm).

#### 4.6. A perforated plate with one edge crack

A perforated plate with 30 holes of diameter 10 mm and one 10 mm long edge crack, as shown in Fig. 14, is analyzed under a tension load of 10 MPa on the top. The plate is simply supported on the bottom. The Young's modulus is 72 GPa, Poisson's ratio is 0.33, fracture toughness is  $3288.76 \text{ N/mm}^{1.5}$  and  $\Delta a_{\max}$  is 0.6 mm. The initial mesh has 6900 elements with 200 elements on each hole and 100 elements on the crack. Fig. 15 shows the results of the crack propagation path using both the FMM BEM and conventional BEM. For the FMM BEM it takes 23 min (total elapsed time) to finish the calculation for 100

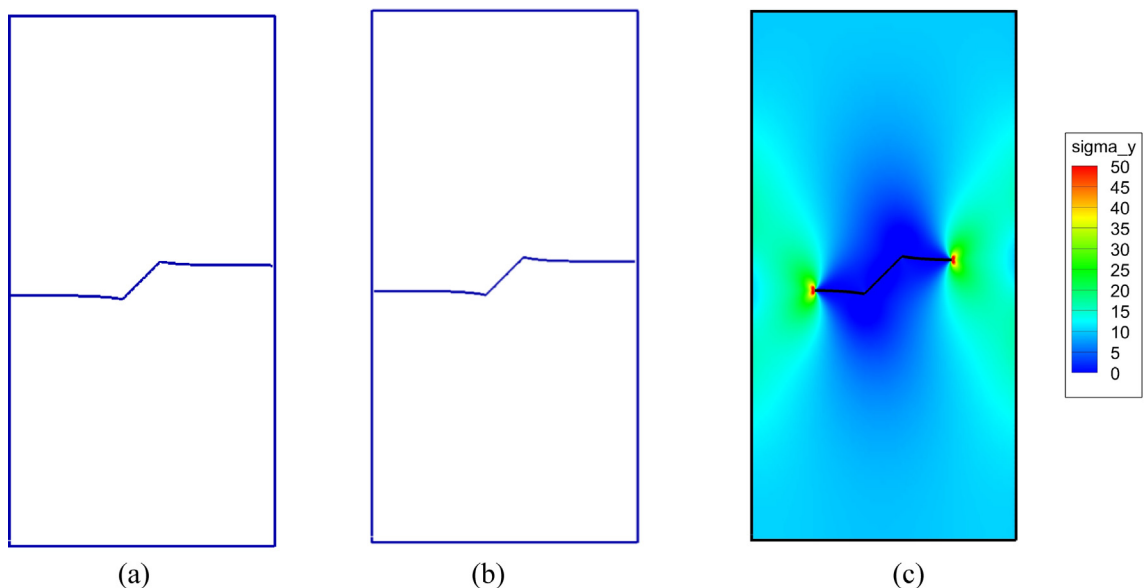


**Fig. 5.** Crack propagation path of the plate with a center crack: (a) FMM BEM; (b) conventional BEM; and (c) stress contour plot (after 16 increments).

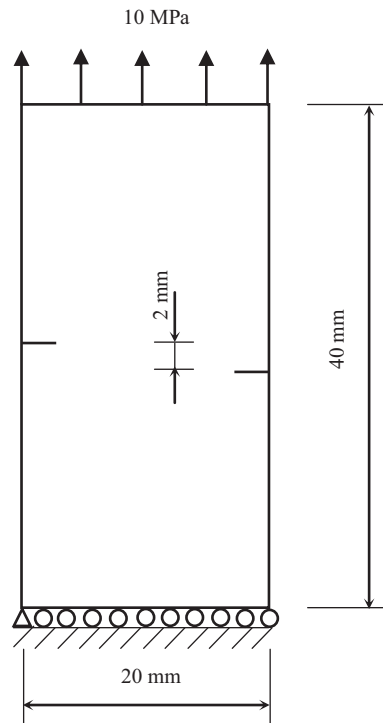


Fig. 6. A plate with two edge cracks (length of 2 mm).

increments (Fig. 15a), while for the conventional BEM it takes 30 min to finish the calculation for 100 increments (Fig. 15b), on the Dell XPS 8900 desktop PC. The final crack propagation path was obtained using the FMM BEM (Fig. 15c), which is bended downward slightly. This may due to the fact that the boundary conditions are not symmetric about the center line in the vertical direction, although the geometry is symmetric.

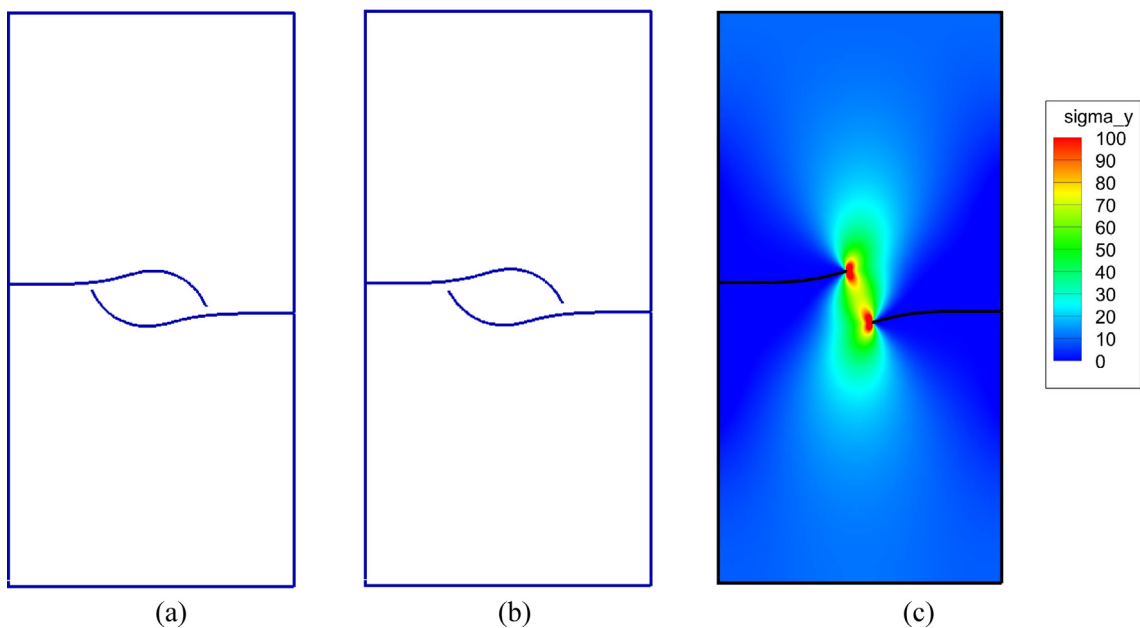
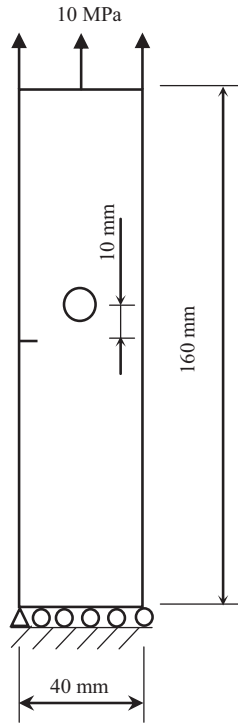


Fig. 7. Crack propagation path of the plate with two edge cracks: (a) FMM BEM; (b) conventional BEM; and (c) stress contour plot (after 27 increments).



**Fig. 8.** A plate with one hole (radius of 5 mm) and one edge crack (length of 6 mm).

#### 4.7. A perforated plate with two edge cracks

In this example, the setup is the same as the previous one, except for the position and number of cracks. Two cracks are located on the edges of two holes as shown in Fig. 16. Fig. 17 shows the results of the crack propagation paths after 45 increments using both the FMM BEM and conventional BEM. The wall-clock times used for solving the models with the FMM BEM and conventional BEM are 9 min and 15 min, respectively.

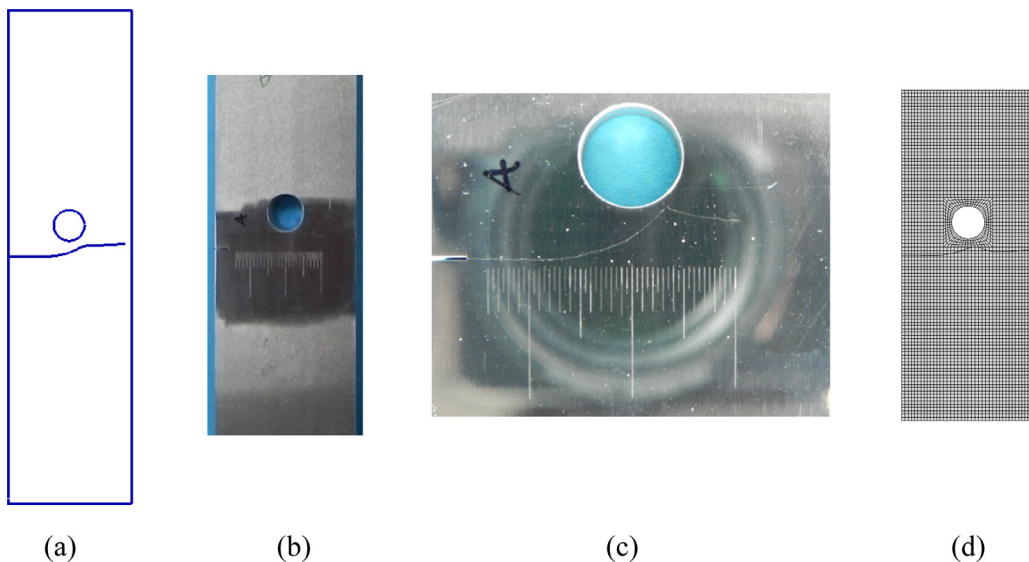


**Fig. 9.** Crack propagation path of the cracked plate with one hole: (a) FMM BEM result (after 45 increments); (b) test sample [59]; (c) test result [59]; (d) XFEM result [59].

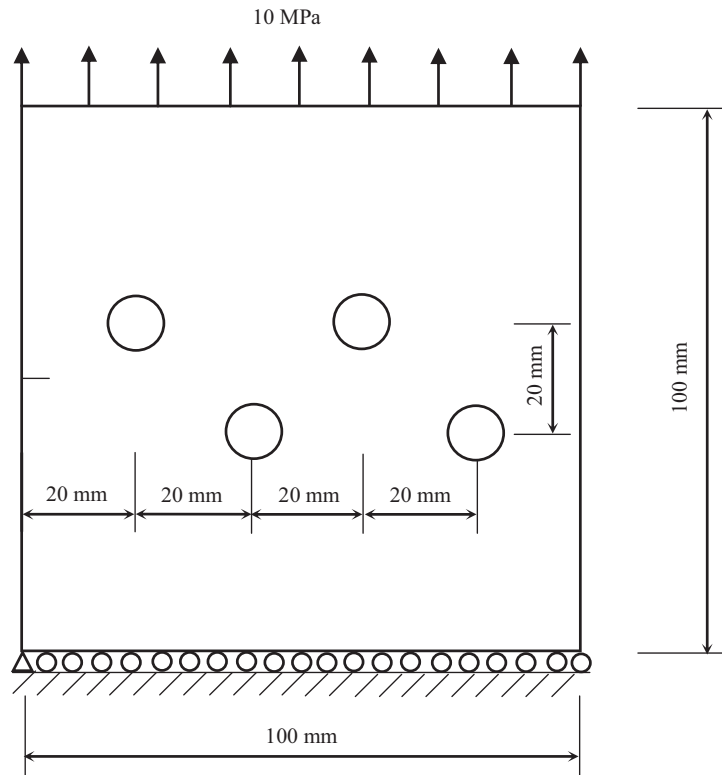


**Fig. 10.** A plate with four holes (radius of 5 mm) and one edge crack (length of 6 mm).

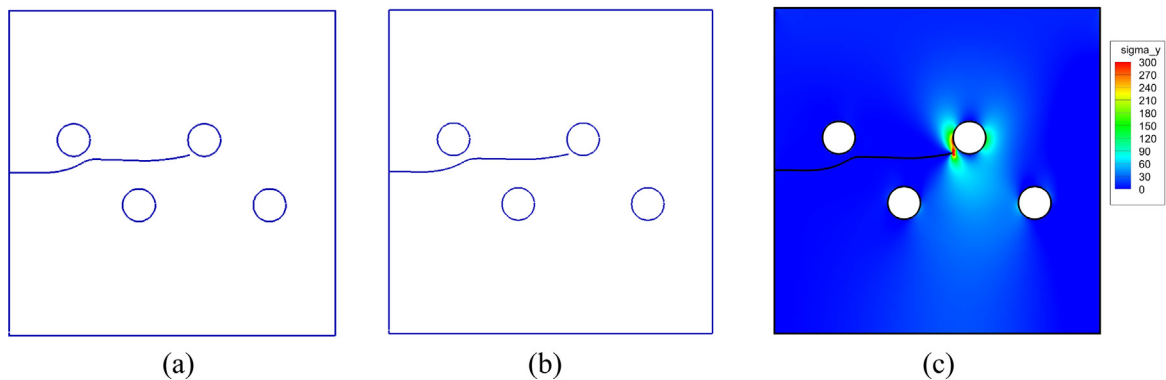


**Fig. 11.** Crack propagation path of the cracked plate with four holes: (a) FMM BEM; (b) conventional BEM; and (c) stress contour plot (after 68 increments).

#### 4.8. A perforated plate with three edge cracks

A perforated plate with 110 holes of diameter 10 mm and three 10 mm long edge cracks, as shown in Fig. 18, is considered next. The plate is subjected to tension of 100 MPa on the top edge and supported on the bottom edge. The Young's modulus is 2.1 GPa, Poisson's ratio is 0.3, fracture toughness is  $3288.76 \text{ N/mm}^{1.5}$  and  $\Delta a_{\max}$  is 0.5 mm. The value of  $m$  in the Paris law and used Eq. (16) is set at 2. The mesh has 23900 elements with 200 elements on each hole and 100 elements on each crack. The effective stress intensity factor exceeds the material toughness at 224 increment and the program stops using 227 min of wall-clock time. Fig. 19 shows the final crack propagation paths calculated by the FMM BEM. The conventional BEM cannot solve the model because of memory size of the PC used.

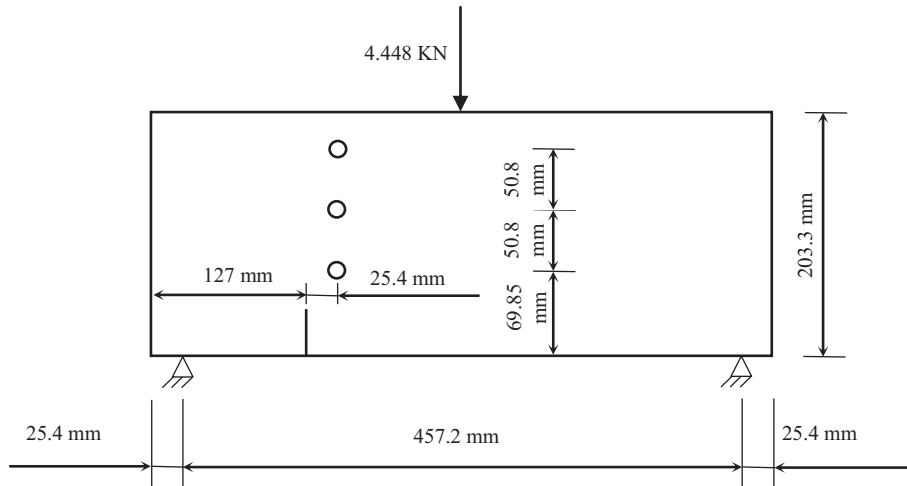


Fig. 12. A plate with three holes (diameter of 12.7 mm) and one edge crack (length of 38.1 mm) and under a bending load [56,57].

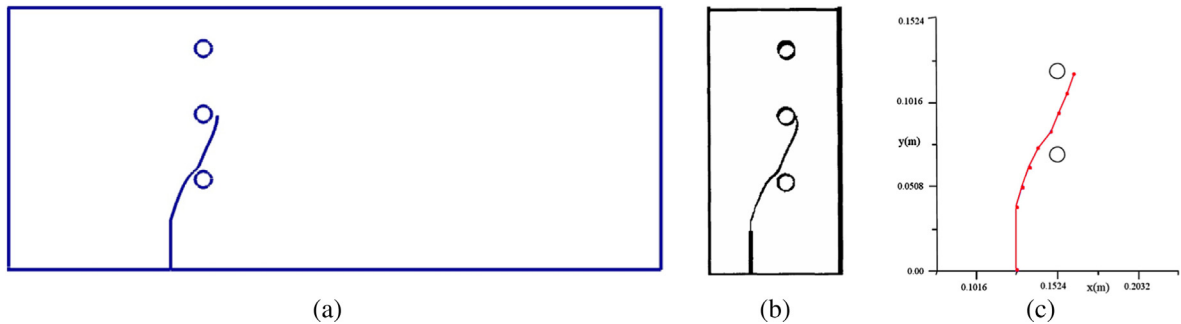


Fig. 13. Crack propagation path of the cracked plate with three holes: (a) FMM BEM result; (b) test result [56,57]; (d) conventional BEM result [56,57].

#### 4.9. Multiple randomly distributed and oriented cracks in an infinite domain

Finally, 100 cracks which are randomly distributed inside a square region in the 2-D infinite domain (Fig. 20) are considered to show the capability of fast multipole BEM in dealing with multiple cracks. The crack length is 20 mm for all cracks. The size of the square region is 800 mm by 800 mm. A remote tension load of 10 MPa is applied in the vertical direction. For the domain, the Young's modulus is 2.1 GPa, Poisson's ratio is 0.3, material toughness is  $3288.76 \text{ N/mm}^{1.5}$ ,  $m = 2$ , and  $\Delta a_{\max}$  is 1.2 mm. There are 100 elements on each cracks; 10000 elements in total. Fig. 21 shows the results of 100 increments using the FMM BEM and obtained with a total elapsed time of 5 h 33 min on the Dell XPS 8900 desktop PC. It is noticed that some of the cracks which are almost parallel to the load direction do not propagate in this case, while those perpendicular to the load direction propagate the most.

## 5. Discussions

A fast multipole BEM for solving 2-D multiple crack propagation problems is presented in this paper. The BEM is based on a dual BIE formulation which uses a linear combination of the displacement BIE and the traction BIE. This dual BIE formulation is applied on all the boundaries of the problem domain and therefore it is easier to implement and use in practice. An adaptive approach is applied in determining the coupling coefficient in this dual BIE formulation, which can provide better conditioning for the BEM system of equations. Constant line elements are applied to discretize the BIE equations (which is equivalent to the DDM [18,19,21]). The developed method is validated or verified by using several example problems. The fast multipole BEM results are compared with either experimental results or other FEM/BEM results. Good agreements among these results are observed in the simple cases studied. For the cases with more complicated geometries, the fast multipole BEM results are also deemed reasonable. The developed program (**FastBEM Fracture 2-D**) available online can be downloaded and used by researchers and engineers to apply this new BEM tool to determine SIFs and to predict the propagation paths of multiple cracks in 2-D elastic domains.

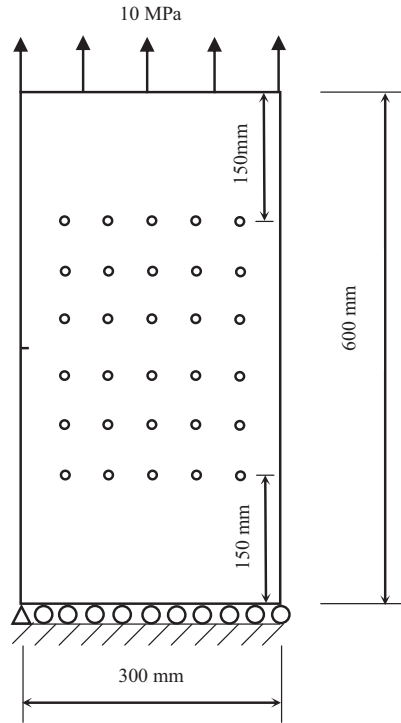


Fig. 14. A perforated plate with one edge crack (radius of holes = 5 mm and crack length = 10 mm).

It is true that more constant elements on each crack surface are needed in modeling crack problems, as compared with quadratic elements commonly used in the BEM. Good results in modeling cracks have been shown in Ref. [45] for computing the SIFs and in this paper for predicting the crack propagation paths using constant elements. The increased cost with more DOFs in using constant elements is offset by the simplicity and efficiency of the developed BEM code, since all integrals (non-singular, nearly-singular, singular and hypersingular ones) are evaluated using analytical integration results [37]. In modeling multiple crack interaction problems, it is very likely to have many nearly-singular integrals where the collocation points are close to elements of integration, which demand delicate and special treatments in the code if quadratic elements are used. Furthermore, the smoothness requirement [52] on using the traction BIE is satisfied automatically by using constant elements, and no corner problems need to be dealt with in the BEM code. All these features of using constant elements and the dual BIE formulation make the fast multipole BEM and its parallel implementation especially effective and efficient.

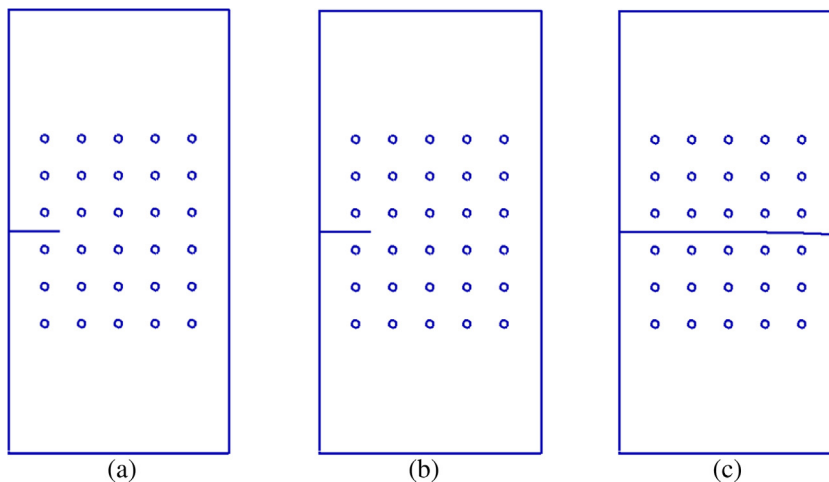
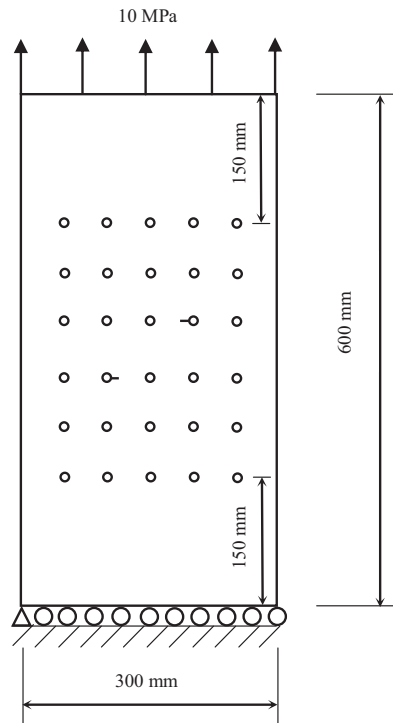
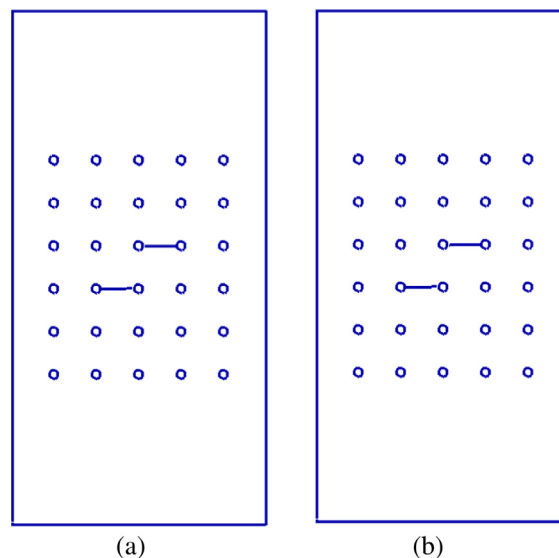


Fig. 15. Crack propagation path of the perforated plate with one edge crack: (a) after 100 increments, FMM BEM; (b) after 100 increments, conventional BEM; (c) after 483 increments, FMM BEM.



**Fig. 16.** A perforated plate with two edge cracks on the holes (radius of holes = 5 mm and crack length = 10 mm).

One can certainly implement quadratic or other higher-order elements to further improve the accuracy of the BEM. However, the efficiency of the BEM will suffer due to the need to deal with special situations like corner problems and singular and nearly-singular integrals (for which analytical integration results are not available yet, in general). Furthermore, in order to meet the smoothness requirement on the traction BIE, some form of the non-conforming elements [13,15,26] will need to be applied, which can no longer guarantee the continuity of the fields between two adjacent elements, similar to the case with constant elements. Therefore, the expected effectiveness and efficiency of using higher-order elements in this case is compromised. Just like the DDM, the BEM with constant elements is believed to be a simpler, more effective and efficient



**Fig. 17.** Crack propagation path of the perforated plate with two edge cracks: (a) FMM BEM; (b) conventional BEM.

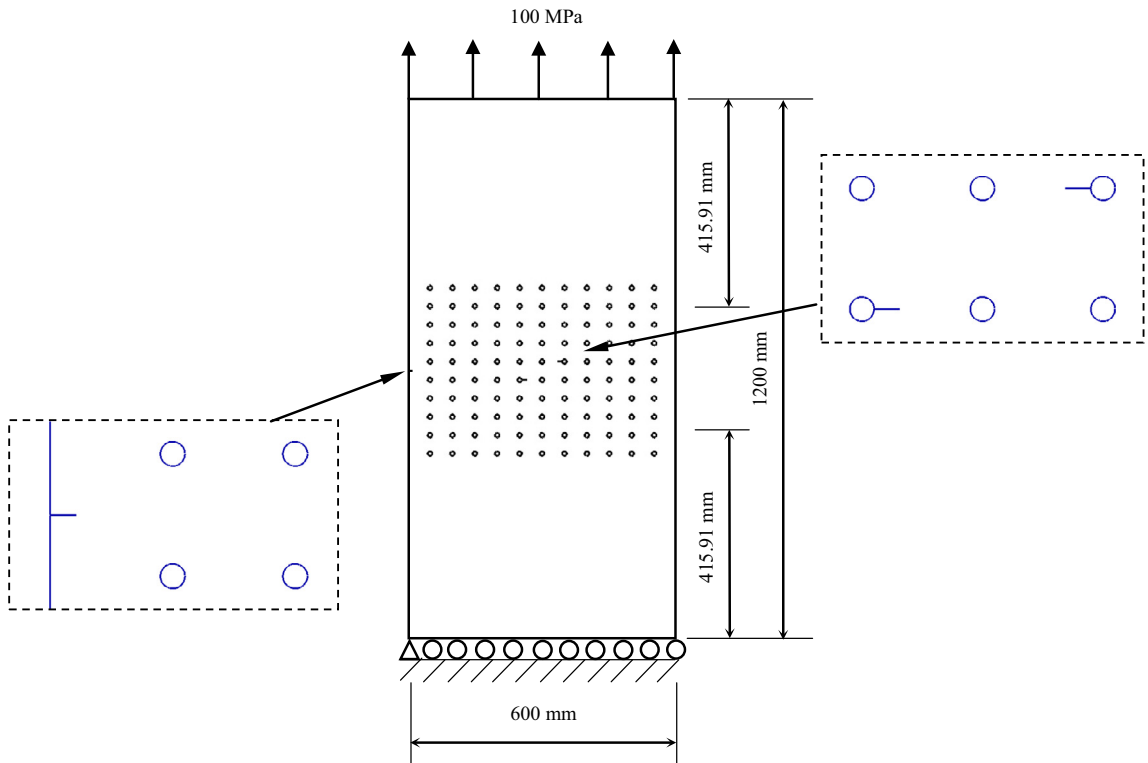


Fig. 18. A perforated plate with three edge cracks (radius of holes = 5 mm and crack length = 10 mm).

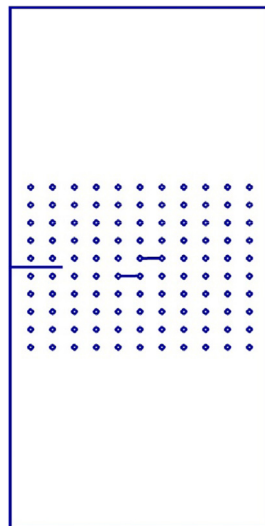
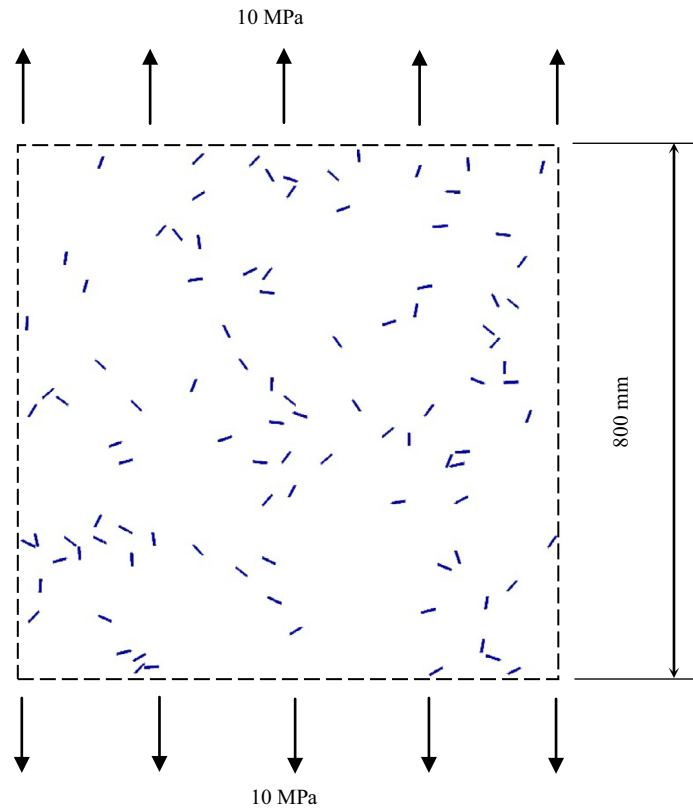


Fig. 19. Crack propagation paths of the perforated plate with three edge cracks (after 224 increments, FMM BEM).

tool for modeling crack problems, as long as a sufficient number of elements are used and a fast solution method for the BEM is employed.

To improve the solution efficiency of the developed BEM, other fast solution methods, such as the adaptive cross approximation (ACA) [60,61] and fast direct solvers can be applied to solve the dual BIE formulations for crack problems. Parallel computing techniques can also be implemented in the code to speed up the solutions on multicore CPU machines and clusters. Extension of the fast multipole BEM to modeling of propagations of multiple cracks in 3-D elastic solids is underway and the results will be reported in a subsequent paper.



**Fig. 20.** Multiple randomly distributed and oriented cracks in an infinite domain (100 cracks of length 20 mm).

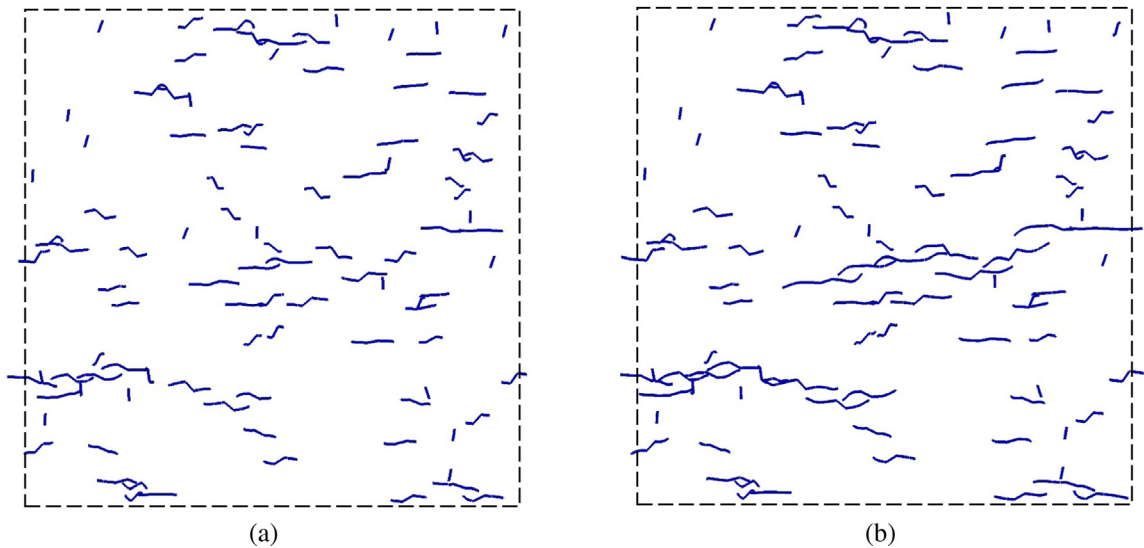


**Fig. 21.** Crack propagation path of the multiple cracks in the infinite domain: (a) after 50 increment steps; (b) after 100 increment steps.

### Acknowledgment

The first and third authors (YJL and WX) would like to acknowledge the funding of the National Natural Science Foundation of China (Project No. 11472218 and No. 11672238) to Northwestern Polytechnical University for supporting this

research project. The authors also thank the three reviewers for their constructive comments and suggestions that have helped improve the final version of the paper.

## References

- [1] Rizzo FJ. An integral equation approach to boundary value problems of classical elastostatics. *Quart Appl Math* 1967;25:83–95.
- [2] Mukherjee S. *Boundary element methods in creep and fracture*. New York: Applied Science Publishers; 1982.
- [3] Sladek V, Sladek J, Balas J. Boundary integral formulation of crack problems. *ZAMM (Z Angew Math Mech)* 1986;66:83–94.
- [4] Cruse TA. *Boundary element analysis in computational fracture mechanics*. Dordrecht, The Netherlands: Kluwer Academic Publishers; 1988.
- [5] Cruse TA. BIE fracture mechanics analysis: 25 years of developments. *Comput Mech* 1996;18:1–11.
- [6] Aliabadi MH. Boundary element formulations in fracture mechanics. *Appl Mech Rev* 1997;50:83–96.
- [7] Aliabadi MH. *The boundary element method – applications in solids and structures*. Chichester: Wiley; 2002.
- [8] Inghraffa AR. *Computational fracture mechanics*. In: Stein E, Borst RD, Hughes TJR, editors. *Encyclopedia of computational mechanics*. West Sussex, UK: John Wiley and Sons; 2008 [Vol. 2, Chapter 11].
- [9] Liu YJ, Mukherjee S, Nishimura N, Schanz M, Ye W, Sutradhar A, et al. Recent advances and emerging applications of the boundary element method. *Appl Mech Rev* 2011;64:1–38.
- [10] Blandford GE, Inghraffa AR, Liggett JA. Two-dimensional stress intensity factor computations using the boundary element method. *Int J Numer Meth Eng* 1981;17:387–404.
- [11] Martin PA, Rizzo FJ. On the boundary integral equations for crack problems. *Proc Royal Soc Lond A* 1989;421:341–55.
- [12] Gray LJ, Martha LF, Inghraffa AR. Hypersingular integrals in boundary element fracture analysis. *Int J Numer Meth Eng* 1990;29:1135–58.
- [13] Krishnasamy G, Rudolphi TJ, Scherr LW, Rizzo FJ. Hypersingular boundary integral equations: some applications in acoustic and elastic wave scattering. *J Appl Mech* 1990;57:404–14.
- [14] Krishnasamy G, Rizzo FJ, Rudolphi TJ. Hypersingular boundary integral equations: their occurrence, interpretation, regularization and computation. In: Banerjee PK et al., editors. *Developments in boundary element methods*. London: Elsevier Applied Science Publishers; 1991 [Chapter 7].
- [15] Krishnasamy G, Rizzo FJ, Liu YJ. Some advances in boundary integral methods for wave-scattering from cracks. *Acta Mech* 1992;3(Suppl):55–65.
- [16] Mukherjee S. On boundary integral equations for cracked and for thin bodies. *Math Mech Solids* 2001;6:47–64.
- [17] Phan AV, Gray LJ, Kaplan T. On some benchmark results for the interaction of a crack with a circular inclusion. *J Appl Mech* 2007;74:1282–4.
- [18] Crouch SL. Solution of plane elasticity problems by the displacement discontinuity method. *Int J Numer Meth Eng* 1976;10:301–43.
- [19] Liu YJ, Li YX. Revisit of the equivalence of the displacement discontinuity method and boundary element method for solving crack problems. *Eng Anal Boundary Elem* 2014;47:64–7.
- [20] Mogilevskaya SG. Lost in translation: crack problems in different languages. *Int J Solids Struct* 2014;51:4492–503.
- [21] Liu YJ. On the displacement discontinuity method and the boundary element method for solving 3-D crack problems. *Eng Fract Mech* 2016;164:35–45.
- [22] Hong HK, Chen JT. Derivations of integral equations of elasticity. *J Eng Mech* 1988;114:1028–44.
- [23] Gray LJ. Boundary element method for regions with thin internal cavities. *Eng Anal Boundary Elem* 1989;6:180–4.
- [24] Krishnasamy G, Rizzo FJ, Liu YJ. Scattering of acoustic and elastic waves by crack-like objects: the role of hypersingular integral equations. In: Thompson DO, Chimenti DE, editors. *Review of progress in quantitative nondestructive evaluation*. Brunswick, Maine: Plenum Press; 1991.
- [25] Portela A, Aliabadi MH, Rooke DP. The dual boundary element method: effective implementation for crack problems. *Int J Numer Meth Eng* 1992;33:1269–87.
- [26] Krishnasamy G, Rizzo FJ, Liu YJ. Boundary integral equations for thin bodies. *Int J Numer Meth Eng* 1994;37:107–21.
- [27] Liu YJ, Rizzo FJ. Scattering of elastic waves from thin shapes in three dimensions using the composite boundary integral equation formulation. *J Acoust Soc Am* 1997;102(2):926–32.
- [28] Chen JT, Hong HK. Review of dual boundary element methods with emphasis on hypersingular integrals and divergent series. *Appl Mech Rev* 1999;52:17–33.
- [29] Xiao F, Hui C-Y. A boundary element method for calculating the K field for cracks along a bimaterial interface. *Comput Mech* 1994;15:58–78.
- [30] Sladek J, Sladek V. Boundary element analysis for an interface crack between dissimilar elastoplastic materials. *Comput Mech* 1995;16:396–405.
- [31] Berger JR, Tewary VK. Boundary integral equation formulation for interface cracks in anisotropic materials. *Comput Mech* 1997;20:261–6.
- [32] Liu YJ, Xu N. Modeling of interface cracks in fiber-reinforced composites with the presence of interphases using the boundary element method. *Mech Mater* 2000;32:769–83.
- [33] Paulino GH, Sutradhar A. The simple boundary element method for multiple cracks in functionally graded media governed by potential theory: a three-dimensional Galerkin approach. *Int J Numer Meth Eng* 2006;65:2007–34.
- [34] Rokhlin V. Rapid solution of integral equations of classical potential theory. *J Comput Phys* 1985;60:187–207.
- [35] Greengard LF, Rokhlin V. A fast algorithm for particle simulations. *J Comput Phys* 1987;73:325–48.
- [36] Greengard LF. *The rapid evaluation of potential fields in particle systems*. Cambridge: The MIT Press; 1988.
- [37] Liu YJ. *Fast multipole boundary element method – theory and applications in engineering*. Cambridge: Cambridge University Press; 2009.
- [38] Helsing J. Fast and accurate numerical solution to an elastostatic problem involving ten thousand randomly oriented cracks. *Int J Fract* 1999;100:321–7.
- [39] Nishimura N, Yoshida K, Kobayashi S. A fast multipole boundary integral equation method for crack problems in 3D. *Eng Anal Boundary Elem* 1999;23:97–105.
- [40] Yoshida K, Nishimura N, Kobayashi S. Application of new fast multipole boundary integral equation method to crack problems in 3D. *Eng Anal Boundary Elem* 2001;25:239–47.
- [41] Yoshida K, Nishimura N, Kobayashi S. Application of fast multipole Galerkin boundary integral equation method to crack problems in 3D. *Int J Numer Meth Eng* 2001;50:525–47.
- [42] Lai Y-S, Rodin GJ. Fast boundary element method for three-dimensional solids containing many cracks. *Eng Anal Boundary Elem* 2003;27:845–52.
- [43] Otani Y, Nishimura N. An FMM for periodic boundary value problems for cracks for Helmholtz' equation in 2D. *Int J Numer Meth Eng* 2008;73:381–406.
- [44] Wang HT, Yao ZH. A fast multipole dual boundary element method for the three-dimensional crack problems. *CMES: Compu Model Eng Sci* 2011;72:115–48.
- [45] Guo Z, Liu YJ, Ma H, Huang S. A fast multipole boundary element method for modeling 2-D multiple crack problems with constant elements. *Eng Anal Boundary Elem* 2014;47:1–9.
- [46] Wang P, Yao Z. Fast multipole DBEM analysis of fatigue crack growth. *Comput Mech* 2006;38:223–33.
- [47] Nishimura N. Fast multipole accelerated boundary integral equation methods. *Appl Mech Rev* 2002;55:299–324.
- [48] Liu YJ, Nishimura N. The fast multipole boundary element method for potential problems: a tutorial. *Eng Anal Boundary Elem* 2006;30:371–81.
- [49] Burton AJ, Miller GF. The application of integral equation methods to the numerical solution of some exterior boundary-value problems. *Proc R Soc Lond Ser A* 1971;323:201–10.
- [50] Liu YJ, Rizzo FJ. A weakly-singular form of the hypersingular boundary integral equation applied to 3-D acoustic wave problems. *Comput Methods Appl Mech Eng* 1992;96:271–87.
- [51] Liu YJ, Rizzo FJ. Hypersingular boundary integral equations for radiation and scattering of elastic waves in three dimensions. *Comput Methods Appl Mech Eng* 1993;107:131–44.

- [52] Martin PA, Rizzo FJ. Hypersingular integrals: how smooth must the density be? *Int J Numer Meth Eng* 1996;39:687–704.
- [53] Liu YJ. Analysis of shell-like structures by the boundary element method based on 3-D elasticity: formulation and verification. *Int J Numer Meth Eng* 1998;41:541–58.
- [54] Liu YJ. A new fast multipole boundary element method for solving large-scale two-dimensional elastostatic problems. *Int J Numer Meth Eng* 2006;65:863–81.
- [55] Anderson TL. *Fracture mechanics: fundamentals and applications*. 3rd ed. Boca Raton: CRC Press; 2005.
- [56] Leonel ED, Venturini WS. Dual boundary element formulation applied to analysis of multi-fractured domains. *Eng Anal Boundary Elem* 2010;34:1092–9.
- [57] Leonel ED, Venturini WS. Multiple random crack propagation using a boundary element formulation. *Eng Fract Mech* 2011;78:1077–90.
- [58] Fender ML, Lechenault F, Daniels KE. Universal shapes formed by two interacting cracks. *Phys Rev Lett* 2010;105:125505.
- [59] Varfolomeev I, Burdack M, Moroz S, Siegele D, Kadau K. Fatigue crack growth rates and paths in two planar specimens under mixed mode loading. *Int J Fatigue* 2014;58:12–9.
- [60] Bebendorf M. *Hierarchical matrices: a means to efficiently solve elliptic boundary value problems*. Berlin: Springer-Verlag; 2008.
- [61] Rjasanow S, Steinbach O. *The fast solution of boundary integral equations*. Berlin: Springer; 2007.